X-ray study of the highly ordered smectic phases of *N*-pentyl-*N'*-(*p*-pentyloxyphenyl)piperazine

Z. X. Fan[a]; H. J. Müller[a]; W. Haase[a]

[a] Institut für Physikalische Chemie, Darmstadt, Germany

PLEASE SCROLL DOWN FOR ARTICLE

X-ray study of the highly ordered smectic phases of N-pentyl-N'-(p-pentyloxyphenyl)piperazine

by Z. X. FAN, H. J. MÜLLER and W. HAASE*

Institut für Physikalische Chemie, Petersenstrasse 20,
64287 Darmstadt, Germany

The structures of the highly ordered liquid crystalline smectic phases of N-pentyl-N'-(p-pentyloxyphenyl)piperazine are identified using X-ray diffraction methods. For this compound a phase sequence hexagonal smectic B (S_B)–ortho-rhombic crystalline smectic E (C_E)–monoclinic crystalline smectic H (C_H) is observed for the first time. The changes in structural symmetry at the phase transitions are discussed.

1. Introduction

The structures of mesophases are usually identified using polarizing microscopy [1, 2], miscibility studies [3, 4] and X-ray diffraction methods [5, 6]. In most cases, the last method gives the definitive answers about the structural arrangement in liquid crystalline phases [6–8]. In addition, nuclear magnetic resonance spectroscopy (NMR) [9], dielectric relaxation spectroscopy [10, 11] and Raman spectroscopy [12] can give information concerning the molecular motion in different liquid crystalline phases.

In order to derive the unequivocal lattice structure and the molecular packing in liquid crystalline phases, adequate macroscopic orientation of the liquid crystalline microdomains must be obtained for the X-ray measurements; this can be achieved either on heating a single crystal [13, 14] or better on cooling down from a low ordered liquid crystalline phase into the desired phases in the presence of an external magnetic or electric field [15, 16]. Using unoriented samples, it is in general difficult to identify the indices of the reflection spots [17].

In the past, the structures of many highly ordered liquid crystalline smectic phases were fundamentally characterized using the flat film X-ray photographic technique. Recently, due to the rapid development of higher resolution X-ray diffraction techniques, a new possibility for performing structural investigations of the highly ordered liquid crystals exists.

In this paper, an attempt is made to solve the structures of the highly ordered liquid crystalline phases for the compound N-pentyl-N'-(p-pentyloxyphenyl)piperazine from the higher resolution diffraction data for the unoriented sample.

2. Experimental

The sample N-pentyl-N'-(p-pentyloxyphenyl)piperazine was synthesized by Dr Bartulin (Departamento de Qumica, Facultad de Ciencias, Universidad de
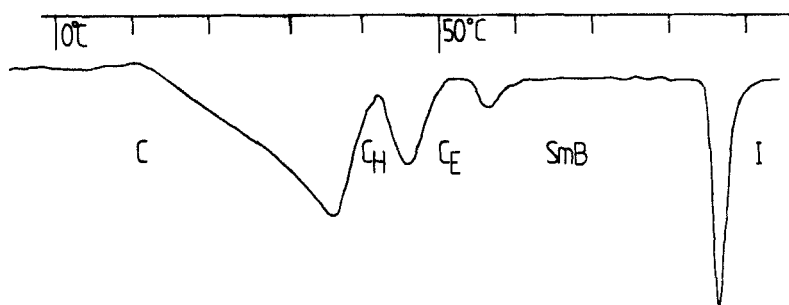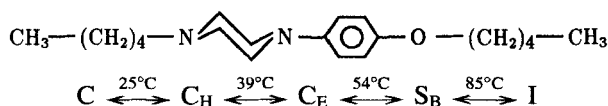
---

* Author for correspondence.

Figure 1.   DSC curve of the first heating process (the sample used had been crystallized from a saturated solution in acetone at $-15°C$).

Concepcion, Chile). Its chemical structure and the phase behaviour are given below:

$$CH_3-(CH_2)_4-N \diagdown N-\langle O \rangle - O - (CH_2)_4 - CH_3$$

$$C \xleftrightarrow{25°C} C_H \xleftrightarrow{39°C} C_E \xleftrightarrow{54°C} S_B \xleftrightarrow{85°C} I$$

DSC measurements show that the phase transition solid–C_H can only be seen using a sample crystallized from a saturated solution in acetone at $-15°C$. On second heating process, the first melting peak for the phase transition solid–C_H disappears. A similar behaviour was also found by polarizing microscopic observations. This indicates the existence of a supercooled C_H phase after the first heating. In figure 1, the DSC curve of the first heating process is plotted. The exact phase transition temperatures were confirmed using polarizing microscopy.

For the X-ray measurements, the sample was put into a Lindemann capillary with a diameter of 1 mm. The capillary was mounted within a self-built oven. The oven temperature was controlled by a regulator (Thor-PID) with an accuracy of $±0.01$ K in the vicinity of the sample. Within the oven, two permanent magnets were installed in a magnetic ring, producing a magnetic field (1 Tesla) through the sample. However, after applying the magnetic field for some days to the liquid crystal phases of the sample, no orientation effect could be detected. For this reason the X-ray diffraction measurements were performed only on the unoriented compound.

A focusing, horizontal two-circle X-ray diffractometer (STOE STADI 2) with a long, fine focus X-ray tube SIEMENS FK (line focus of $0.4 × 12$ mm^2) as X-ray source was used for the higher resolution X-ray data collection. The $CuK\alpha_1$ radiation ($\lambda = 1.54056$ Å) was focused by a curved Ge(111) monochromator. The mechanical and electrically controlled smallest stepwidth of the diffractometer was $0.001°$ in 2θ and ω. For fast diffractometry, a linear position-sensitive detector (STOE Mini PSD) was used with a resolution of the stepwidth of $0.01°$ in 2θ. The X-ray measurements were done using transmission geometry. A detailed description of the experimental set-up has been reported in [18].

3.   Results and discussion

As mentioned above, it is impossible to align the compound in a magnetic field (~ 1 Tesla), because no nematic or smectic A phases exist above the S_B phase.
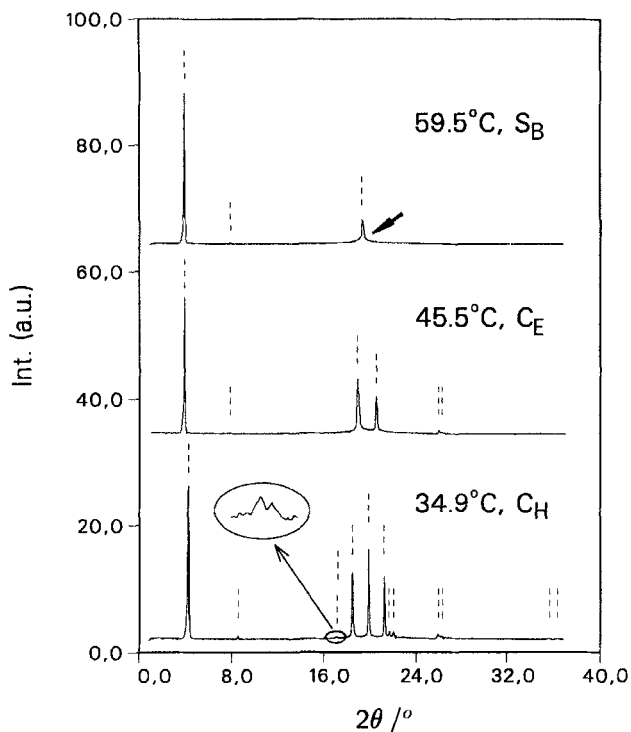
Figure 2. The one-dimensional scattering diagrams in the different liquid crystalline phases; the arrow shows the arched background scattering in the S_B phase.

Figure 2 shows the 2θ-scan for unoriented sample in the different smectic liquid crystalline phases.

The peak positions were extracted from the scattering profiles using the 'STADI powder software' [19]. Using the same program, the primary index characterization was made from the four strongest peaks following standard definition for orthorhombic and monoclinic systems [20], with the exception of the hexagonal S_B phase. The logic solution was used in consideration of conditions limited for possible reflections. The best fitting results are listed in table 1.

In order to distinguish the solid phase from the C_H phase, a single crystal analysis was performed on a suitable flat prism obtained by recrystallization from a saturated solution in acetone at − 15°C. The intensity measurements were made at 22°C on an automatic four-circle diffractometer (STOE-Siemens AED2) with graphite mono-chromated CuK_α radiation ($\lambda = 1.54178$ Å). The lattice dimension was determined by a least-squares refinement of 16 strong reflections. The crystal data are listed in table 2.

Unequivocal structural differences can be seen between the unit cells of the solid phase and the C_H phase (Crystalline smectic H—see table 1). Because of the strong thermal fluctuations, it is impossible to fix all geometric positions, but structure analysis at low temperatures is at present in process.

Using a MNDO program [21], we have simulated the favoured configuration of the molecule investigated. In figure 3, this is shown viewed in two orthogonal directions. It is found that the average distance between the two end methyl groups, including the

Table 1. Index identification and the elementary cell for the S_B, C_E and C_H phases.

2θ/° (exp.)	2θ/° (calc.)	d/Å (exp.)	d/Å (calc.)	Δd/d per cent	h k l	Int.†	Cell	
				Hexagonal smectic B phase at 59.3°C				
3·920	3·934	22·522	22·443	0·35	0 0 1	s	a	5·30 Å
7·881	7·867	11·209	11·228	−0·17	0 0 2	vw	c	22·44 Å
19·24		4·608‡			1 0 0	n	V	554·9 Å³
				Orthorhombic crystalline smectic E phase at 45.2°C				
3·930	3·935	22·464	22·435	0·13	0 0 1	s	a	8·67 Å
7·886	7·875	11·202	11·218	−0·14	0 0 2	vw	b	5·59 Å
18·856	18·875	4·702	4·698	0·09	1 1 0	m	c	22·44 Å
20·463	20·461	4·336	4·337	−0·02	2 0 0	m	V	1087 Å³
25·956	25·985	3·430	3·426	0·12	2 1 0	w		
26·234	26·292	3·394	3·387	0·21	2 1 1	vw		
				Monoclinic crystalline smectic H phase at 34.9°C				
4·238	4·275	20·832	20·654	0·86	1 0 0	s	c	9·81 Å
8·541	8·555	10·344	10·327	0·16	2 0 0	w	b	5·32 Å
17·142	17·159	5·168	5·163	0·10	4 0 0	vw	a	22·59 Å
17·193	17·195	5·153	5·152	0·02	1 1 0	vw	β	113·9°
18·471	18·451	4·799	4·805	−0·12	1 0 $\bar{2}$	m	V	1078 Å³
19·780	19·780	4·485	4·485	0·00	0 0 2	m		
21·081	21·084	4·211	4·210	0·02	3 1 0	m		
21·505	21·494	4·128	4·131	−0·07	5 0 0	w		
21·895	21·899	4·056	4·055	0·02	1 0 2	w		
25·870	25·962	3·441	3·429	0·35	0 1 2	w		
26·292	26·350	3·386	3·379	0·21	4 1 $\bar{2}$	w		
35·633	35·603	2·518	2·520	−0·08	4 1 2	w		
36·254	36·215	2·476	2·478	−0·08	8 1 $\bar{1}$	w		

† s = strong; m = medium; w = weak; vw = very weak.

‡ for hexagonal system $d_{100} = d_{010} = d_{0\bar{1}0} = d_{\bar{1}00} = d_{\bar{1}10} = d_{1\bar{1}0}$ and $a = b$.

Table 2. Crystal data for the solid phase.

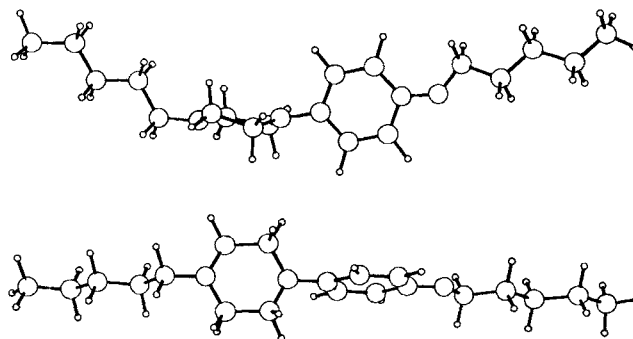| Temp.	a	b	c	β	Volume	Space group
22·0°C	12·044	8·125	43·01	104·9°	4008·7	$P2_1/c$

Figure 3. Molecular configuration calculated using a MNDO program, viewed from two orthogonal directions.

van der Waal's radius, amounts to 22·58 Å, which is nearly identical with the layer thickness in the S_B, as well as the C_E phases (see table 1).

Looking at the scattering profile for the hexagonal S_B phase, one finds two strong reflections with maximum positions at 3·920 and 19·244° in 2θ. The d-value of the inner reflection (22·44 Å) is approximately equal to the molecular length. This indicates that the molecules are arranged perpendicularly to the smectic layers. The single outer reflection gives evidence for a hexagonal molecular packing within the smectic layer. Because of the lack of three-dimensional scattering reflection for the S_B phase, we cannot recognize exactly whether it concerns a three-dimensional crystalline smectic B phase and conclude temporally that it is a two-dimensional hexagonal smectic B structure.

In contrast to the inner (001)-reflection, the intensity of the (002)-reflection at 7·881° is very weak. This convinces us of a fluctuating smectic structure. Moreover, the so-called hexagonal packing means only a pseudohexagonal packing with strong molecular motion, including molecular rotation around the molecular long axis and vibration about an equilibrium position. In this case, an arched background scattering is found close to the outer reflection as shown in figure 2—see arrow in figure.

It must be pointed out here that the length of the c axis in the S_B phase (22·44 Å) means only that there is an average thickness of the smectic layer. In this case, the corresponding cell volume means only a volume of a hexagonal packing with a certain thickness.

In relation to the hexagonal S_B phase, the orthorhombic C_E phase is realized through a freezing of the molecular rotation from a cylinder-like molecular form to a elliptically-shaped molecular form (see figure 4), with the simultaneous extension of one edge and shortening of another edge at the phase transition S_B–C_E. In consequence, the 6-fold rotation axis in the S_B phase disappears, giving a 2-fold rotation axis in the C_E phase. Because the molecular long axis remains perpendicular to the smectic layers
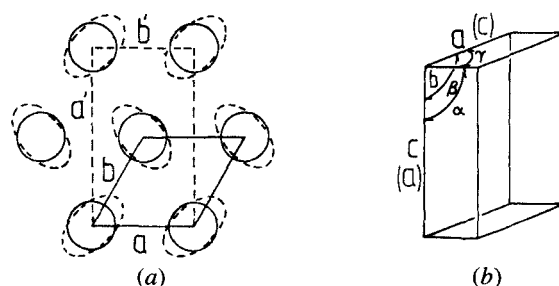
Figure 4.   The changes of the elementary cell at the phase transitions; (*a*) the building of the orthorhombic C_E phase, starting from the hexagonal molecular packing in the S_B phase (solid line and *a*, *b*: hexagonal phase; dashed line and *a'*, *b'*: orthorhombic phase); (*b*) the change of the elementary cell from orthorhombic C_E phase to monoclinic C_H phase, realized through tilting via angle β (the directions of the *a*- and *c*-axes are exchanged one for the other).

in both phases, the change of *d*-value of the inner (001) reflection is of course very small (table 1).

Further cooling converts the C_E phase into the C_H phase. This C_E–C_H phase transition is observed for the first time. But in view of the structural symmetry, it is easy to understand that this phase transition occurs through the orthorhombic cell inclining via the β-angle (figure 4). A C_K phase would be built through a tilting of the cell via the angle α, and be distinguished from the C_E–C_H phase transition. A third possibility, at least theoretically, is a tilting through the angle γ. However, up to now no report concerning the last type of liquid crystalline phase has appeared. It should be pointed out that the C_K and C_H phases are the most crystalline-like liquid crystal phases known.

According to Diele *et al.*, the C_H phase is related to the crystal smectic G phase by loss of molecular rotational freedom and loss of the *c*-centring of the unit cell [16].This results in a monoclinic symmetry by the adoption of a 'herringbone'-packing with a tilt angle along the side edge. Leadbetter *et al.*, have pointed out that in so-called 'herringbone' phases, the molecules remains disordered with respect to rotation about both the long and short molecular axes [22].

As demonstrated in table 1, the C_E and C_H phases show crystal-like behaviour with crystal analogue net planes (C_E: (211); C_H: (412), (41$\bar{2}$) and (81$\bar{1}$)). But at wide angle (> 37°) no reflections related to molecular packing can be found. This indicates that the strong incommensurable molecular fluctuations which effectively lead to smoothing of the scattering planes. Beside this, the scattering intensities associated with the normal line of the smectic layers, but with high indices, i.e. the (00*l*) reflections for the S_B and C_E phases and the (*l*00) reflections for the C_H phase, are without exception very weak, resulting from undulation of the smectic layer. This is the reason why we talk here about liquid crystalline smectic phases.

In figure 5, the changes of the space group at the phase transitions are plotted. The S_B phase is defined as a two-dimensional space group, P6m [23 (a)], in agreement with the presumption of a two-dimensional S_B structure as mentioned above. In the C_E phase, the *c*-axis is extended along the molecular long axes and the [*hk*0]-plane lies along the smectic layers. However, after the phase transition C_E–C_H, the directions of the *a*- and *c*-axes are exchanged relative to each other in order to follow the standard representation for the space group C_{2h}^5 (P2$_1$/c) [23 (b)].
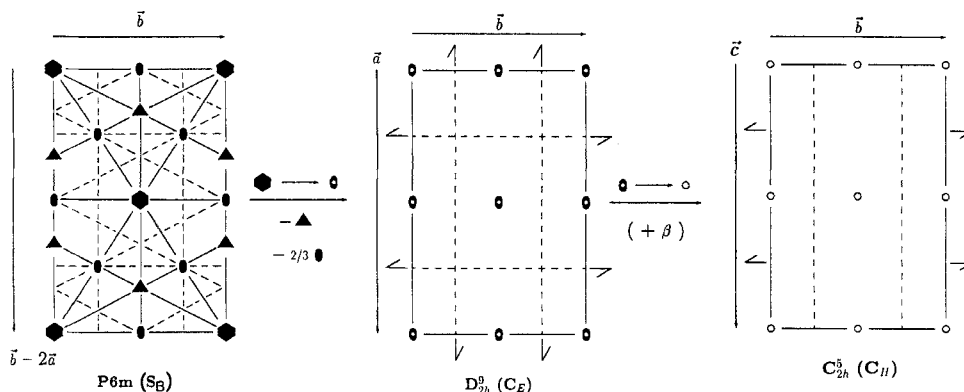
Figure 5. The changes of structural symmetry at the S_B–C_E and C_E–C_H phase transitions.

According to dielectric investigations, the activation energies for reorientation around the molecular long axes in the S_B phase are comparable with those in the nematic or S_A phase [10], and such reorientations around the molecular long axes are typical for all liquid crystalline phases. For instance, it has been found that the reorientation of dipole moments around the long axes of a molecule is faster than 10^8 Hz [24] in the crystalline smectic G phase. This is one of the reasons for the decrease in the scattering intensity for reflections with high indices.

References

[1] FRIEDEL, M. G., 1992, *Annln Phys.*, **18**, 273.
[2] DEMUS, D., and RICHTER, L., 1978, *Textures of Liquid Crystals* (Verlag Chemie, Weinheim).
[3] SACKMANN, H., and DEMUS, D., 1969, *Fortschr. chem. Forsch.*, **12**, 349.
[4] GRAY, G. W., and GOODBY, J. W., 1984, *Smectic Liquid Crystals-Textures and Structures* (Leonard Hill).
[5] DE VRIES, A., 1973, *Molec. Crystals liq. Crystals*, **24**, 337.
[6] PERSHAN, P. S. (editor), 1988, *Structure of Liquid Crystal Phases* (and the literature therein) (World Scientific).
[7] DE GENNES, P. G., 1972, *C. r. hebd. Séanc. Acad. Sci., Paris* B, **274**, 2468.
[8] LEADBETTER, A. J., and WRIGHTON, P. G., 1979, *J. Phys., Paris*, **40**, C3-234.
[9] BROWN, G. H., DOANE, J. W., and NEFF, V. D., 1971, *A Review of the Structure and Physical Properties of Liquid Crystals* (LCRC Press).
[10] KRESSE, H., 1982, *Fortschr. Phys.*, **10**, 507.
[11] PFEIFFER, M., WROBEL, S., BERESNEV, L. A., and HAASE, W., 1991, *Molec. Crystals liq. Crystals*, **202**, 193.
[12] JEN, S., CLARK, N. A., PERSHAN, P. S., and PRIESTLEY, E. B., 1977, *J. chem. Phys.*, **66**, 4635.
[13] LEVELUT, A. M., 1976, *J. Phys., Paris*, **37**, C3-51.
[14] BENATTAR, J. J., DOUCET, J., LAMBERT, M., and LEVELUT, A. M., 1979, *Phys. Rev.* A, **20**, 333.
[15] LEADBETTER, A. J., FROST, J. C., and MAZID, M. A., 1979, *J. Phys. Lett., Paris*, **40**, L325.
[16] DIELE, S., BRAND, P. and SACKMANN, H., 1972, *Molec. Crystals liq. Crystals*, **17**, 163.
[17] BELARBI-MASSOURAS, Z., TAKAGI, A., EMA, H., HASEBE, H., OHTA, K., FUJIMOTO, T., and YAMAMOTO, 1991, *Molec. Crystals liq. Crystals*, **201**, 147.

[18] KLÄMKE, W., FAN, Z. X., HAASE, W., MÜLLER, H. J., and GALLARDO, H. O., 1989, *Ber. Bunsenges. phys. Chem.*, **93**, 478.

[19] STOE and CIE GmbH, 1992, STADI powder software (unpublished).

[20] BUERGER, M. J., 1970, *Contemporary Crystallography* (McGraw-Hill).

[21] DEPARTMENT OF CHEMISTRY, Indiana University, 1987, *Quantum Chemistry Program Exchange No. 523, MNDO version 4.01.*

[22] RICHARDSON, R. M., LEADBETTER, A. J., and FROST, J. C., 1982, *Molec. Phys.*, **45**, 1163.

[23] LONSDALE, K. (editor), 1952, *International Tables for X-Ray Crystallography*, Vol. 1 (The Kynoch Press), (a) p. 72; (b) p. 99.

[24] BATA, L., and BUKA, A., 1981, *Molec. Crystals, liq. Crystals*, **63**, 307.